# Reports

## Direct Observation of Global Protein Motion in Hemoglobin and Myoglobin on Picosecond Time Scales

L. GENBERG, L. RICHARD, G. MCLENDON, R. J. DWAYNE MILLER

**Picosecond phase-grating spectroscopy is highly sensitive to density changes and provides a new holographic approach to the study of protein dynamics. Photodissociation of carbon monoxide from heme proteins induces a well-defined transition from a ligated to a deoxy structure that is important to hemoglobin and myoglobin functionality. Grating spectroscopy was used to observe protein-driven density waves on a picosecond time scale after carbon monoxide dissociation. This result demonstrates that global tertiary structure changes of proteins occur on an extremely fast time scale and provides new insight into the biomechanics of deterministic protein motion.**

THE ENERGETICS AND DYNAMICS OF protein motion are key issues in understanding proteins. Hemoglobin (Hb) and myoglobin (Mb) have been studied extensively in this regard, because their structural and spectroscopic features are well characterized. These proteins exhibit large amplitude-correlated structural changes that are associated with the binding and release of small ligands. These processes are particularly amenable to ultrafast optical probes, because the dynamics involved in these processes can be optically triggered. One of the main questions remaining in these systems is the mechanism of energy transduction from a stimulus, such as the dissociation of a ligand, to the specific protein motions associated with the function of the molecule and the dynamics of the protein motion. Because specific motions of proteins necessarily involve the correlated action of a considerable number of atoms, the energy must be directed and distributed over several coordinates in order for the motion to occur. In the heme proteins, the motion to the deoxy structure is triggered by the displacement of the central Fe atom from the porphyrin ring and doming of the ring after ligand dissociation. The resulting change in atom-atom interactions creates potential energy gradients that supply the force to displace the atoms from one structure to another.

In the strain model for this motion (*1*), the whole process is envisaged as a fairly localized change in the potential energy gradients. On going from a ligated to a deoxy structure, the heme doming pushes on the proximal histidine, which rotates and moves away from the ring after dissociation. This motion in turn creates a force that pushes the α helix into the deoxy position. This time-dependent shift in the spatial position of the potential energy gradient is analogous to the sequential falling of dominoes. However, the exact length scale over which the potential energy gradient is delocalized is unknown and needs to be determined by dynamical studies of the protein motion.

The ideal tool for investigating this problem is phase-grating spectroscopy, which has high sensitivity to density changes and picosecond time resolution. In a transient grating experiment, two time-coincident excitation pulses of the same wavelength are brought into the sample and crossed at an angle θ to form an optical interference pattern. This pattern is holographically encoded in the sample through photoprocesses induced by the excitation pulses that change the complex index of refraction of the material. The spatial pattern, or fringe spacing, of the diffraction grating is dependent on the excitation beam geometry (*2*)

$$\Lambda = \frac{\lambda_{ex}}{2 \sin(\theta/2)} \quad (1)$$

where Λ is the grating fringe spacing and $\lambda_{ex}$ is the excitation wavelength. A variably time-delayed probe pulse is brought into the sample at the correct angle for Bragg diffraction from the grating image. For probe wavelengths well off resonance, the diffraction efficiency (η) of the grating is determined by changes in the real part of the index of refraction (*3*). A phase grating develops with

$$\eta = \left(\frac{\pi d}{\lambda_p \cos \phi} \Delta n\right)^2 ; \Delta n = \frac{\partial n}{\partial \rho} \delta\rho \quad (2)$$

where λρ is the probe wavelength, φ is the Bragg diffraction angle, $d$ is the grating thickness, $\Delta n$ is the grating peak-null variation in the index of refraction, and ρ is the density.

As indicated in Eq. 2, the dominant contribution to changes in the index of refraction for liquids is photoinduced changes in the material density. Generally, density changes arise from the thermal expansion of the lattice (which decreases the density) that accompanies the deposition of energy through nonradiative relaxation of excited states (*3–5*). This feature of the spectroscopy has been exploited to study vibrational energy relaxation (*5*), the energetics of photoreactions (*6*), and weak optical absorption in solution (*4*). However, density changes can also be induced by optically triggered changes in molecular volume or conformation. This work takes advantage of the high sensitivity and time resolution of holographic techniques to density changes to follow

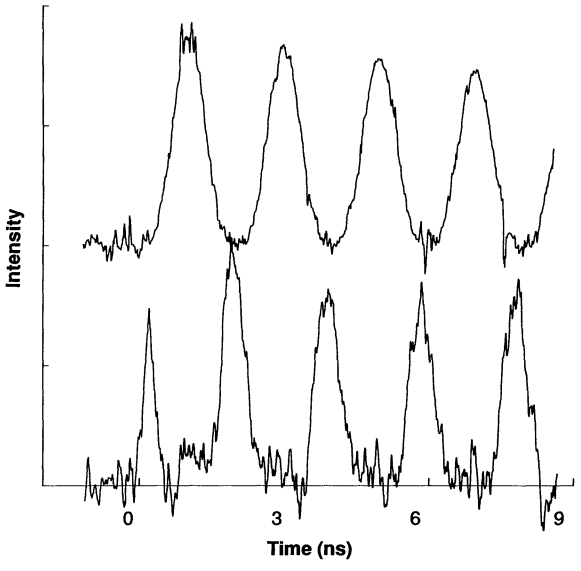


**Fig. 1.** Probe pulse intensity as a function of delay time under low excitation condition, 1.5 mJ/cm² (~10% photodissociation); (**top**) deoxy-Mb; (**bottom**) MbCO.

Department of Chemistry and Institute of Optics, University of Rochester, Rochester, NY 14627.

the dynamics of protein motion. As detailed below, the density changes arise from material displacement that occurs during the course of the optically triggered structure transition of the heme protein. In this case, the dynamics and amplitude of the grating image replicate the protein motion and give a direct measurement of this process.

We conducted picosecond transient phase-grating studies on the ligated-to-deoxy structure transition for both carboxyhemoglobin (HbCO) and carboxymyoglobin (MbCO) by using 532-nm excitation and an off-resonant probe at 1.064 μm. The experimental setup has been described elsewhere (*5*). Excitation at 532 nm dissociates the CO ligand in less than 300 fs (*7, 8*). A fraction of the dissociated CO recombines with the central heme Fe in ~100 ns, and the remaining CO diffuses out of the protein matrix to recombine on a slower time scale (*9–11*). Intermediate to these time scales, the protein undergoes large-amplitude motions that drive the system toward the deoxy heme structure.

Experimental transient phase-grating studies of this structure change in Mb are shown in Fig. 1. The upper curve shows the control study of deoxymyoglobin (deoxy-Mb). These data reflect a purely thermal response. Earlier studies of deoxy-Mb and analogous heme proteins have shown that the absorbed photon energy is deposited into the aqueous bath in less than 20 ps (*5*), in agreement with molecular dynamics calculations (*12*). The optical excitation energy is uniformly redistributed into the large density of vibrational modes of the protein. This prevents coupling to a particular structure coordinate and changes in tertiary structure. The subsequent energy transfer to the water layer and ensuing thermal expansion excites a standing acoustic wave, which beats in time with the acoustic period that depends on $\Lambda$ and the speed of sound in water. The first maximum in the signal in this case is observed at one-half an acoustic period from $t = 0$, as expected for a purely thermal response.

In contrast, the lower curve in Fig. 1 shows the data observed for MbCO under identical conditions. There is an extremely fast rise time in the density-induced change in the index of refraction, and the generated acoustics are 180° out of phase with the strictly thermal response. The observed picosecond dynamics are attributable to changes in the protein structure. The time scale for this density or volume change is determined by the speed at which the protein motion changes the effective volume of the protein. This result gives direct evidence for large-scale global protein motion on a picosecond time scale.

Although not completely discernible from Fig. 1 for MbCO, there are acoustic waves generated by both the protein motion and the thermal expansion. The thermalization of the excess energy above that needed to break the Fe–CO bond and the induced tertiary structure changes are independent processes, and the two contributions are separable on the basis of the grating dynamics. One can determine the sign of the density change driven by the protein transition by comparing the sign of the acoustic strain amplitude to the known positive expansion of the thermal response. We accomplished this comparison by increasing the relative magnitude of the thermal response over the protein wave through two-photon processes (Fig. 2). At high power (Fig. 2A) with ~100% CO dissociation, two-photon absorption processes deposit excess thermal energy into the lattice over the protein response through fast nonradiative relaxation of short-lived, highly excited MbCO and deoxy-Mb electronic states (*5, 13*). The normal thermal acoustic grating response dominates the signal under these conditions. As the excitation conditions are lowered (Fig. 2B), a double beating is observed between the thermal response and the protein wave. This double oscillation in the signal and narrowing of the peak widths demonstrates that the two acoustic responses are opposite in sign in their effect on the water density. At low-excitation conditions, with less than 10% photodissociation (Fig. 2C), the protein-driven wave dominates, as shown in Fig. 1. The opposing behavior of the protein-driven wave relative to the thermal wave is consistent with the protein springing open as it undergoes its tertiary structure change.

In addition to the above evidence, the magnitude of this protein response differs between the Mb and Hb proteins (Fig. 3). Relative to MbCO, HbCO has a 1.5 to 2 times smaller amplitude for the protein displacement wave under the same excitation conditions per heme, and the thermally driven acoustics dominate. The protein-driven acoustics are discernible as the small-amplitude oscillations in the signal that have the same rise time and phase as the MbCO acoustics. The difference in the amplitude of the protein-driven acoustics is attributed to the difference in quaternary structure of the two proteins. The tetrameric structure and subunit interaction of HbCO constrain the motion of a single subunit as it undergoes its tertiary structure change. This interaction would be absent for the monomeric MbCO proteins. The inertial mechanical constraint imposed by the quaternary structure is an important component to the strain model of cooperativity in Hb (*1, 14*).

In addition to the deoxy-Hb studies, oxyhemoglobin ($HbO_2$) was also used as a

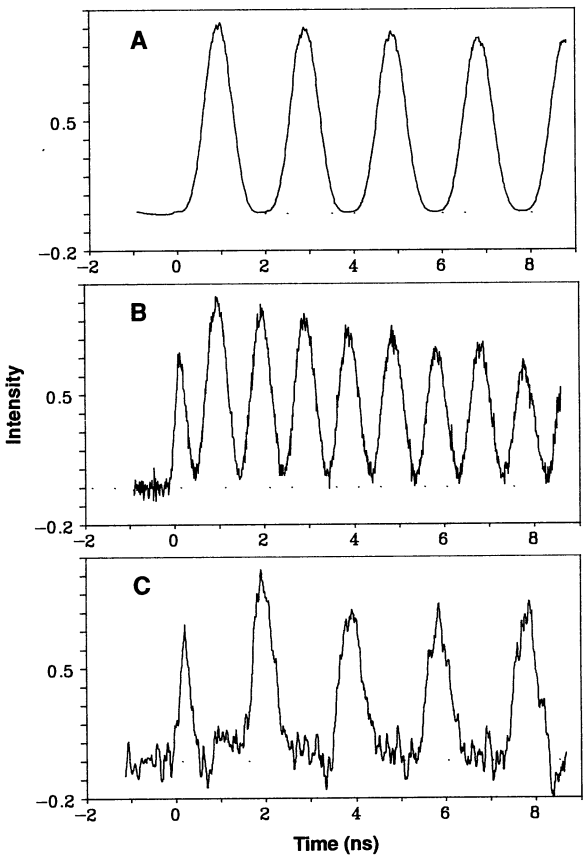


**Fig. 2.** A power dependence of the grating signal for MbCO at a 1064-nm probe wavelength with $\theta$ = 10°: (**A**) high-excitation conditions (39 mJ/cm$^2$); (**B**) intermediate power (6.5 mJ/cm$^2$); and (**C**) low-excitation conditions (1.5 mJ/cm$^2$).

control. This system serves as a better control, because there are negligible structure differences and both ligands undergo photodissociation. Earlier work has established that $O_2$ photodissociates with ~100% quantum yield like CO, but most (~70%) of the $O_2$ recombines with the central Fe atom in less than 5 ps (*7*). Of the remaining photoproduct, approximately one-half geminately recombines on the 200-ps time scale (*6, 15*). This rapid recombination would return the protein to the ligated structure and thereby turn off the protein displacement before it could contribute to the signal. If we take into account the quadratic scaling of the signal and note that the $O_2$ recombination dynamics are convolved to the laser pulse durations (100 ps), the protein signal should be reduced by more than an order of magnitude relative to that of HbCO. The $HbO_2$ results are shown in the upper part of Fig. 3 as a dashed curve. In this case, the protein wave was not observed, which, within our signal to noise ratio, indicates that the protein wave driven by $O_2$ photodissociation was only 1/7 the amplitude of that for CO, as expected. In addition, the amount of energy thermalized is increased by the $O_2$ recombination. This further increases the response of the thermal grating component by approximately a factor of 4 over that of the protein-driven component such that only the thermal grating response is observed.

To completely rule out any type of thermal acoustic artifact unrelated to the protein dynamics, we performed control studies near 4°C, the zero thermal expansion point for pure water, on all of the proteins (Fig. 4). For the protein solutions, the freezing point of water is lowered and the zero thermal expansion point is shifted to ~0°C (*10*). At −0.3°C, the thermal acoustic wave amplitude for deoxy-Mb is reduced by more than a factor of 100. In contrast, the amplitude of the protein-driven displacement wave remains relatively constant as the system goes from room temperature to −0.3°C. Similar results were obtained for the Hb proteins, although the amplitude of the thermal component to the HbCO data did not reduce as much as that of the deoxy-Hb control. These results demonstrate that the acoustics associated with the CO photodissociation of heme proteins are not thermal in nature and must be assigned to material displacement driven by the optically triggered structure changes.

The time scale over which these global motions occur is important in establishing the mechanism for the protein motion. These results demonstrate that a large-amplitude correlated structure change occurs within 30 ps after CO dissociation (inset to Fig. 4). Earlier work by a number of groups has demonstrated that tertiary structure changes in the vicinity of the heme group, involving the proximal histidine or porphyrin ring, occur in less than 30 ps for Mb and a fast component (less than 30 ps) followed by slower relaxation components for Hb (*7, 9, 16, 17*). Our studies are in agreement with the results of this earlier work. The present study demonstrates that not only has the protein undergone local structure changes near the epicenter for the structure transition but also global, collective changes on this time scale.

These results reveal that dissociation of CO leads to a large change in the potential energy surface of the protein. The nature of the observed response gives direct evidence that this change sets up potential energy gradients that act as a uniform force to collectively displace a large number of atoms. This observation supports the model of stored strain energy as the driving force of protein motion. However, the potential energy gradients would have to be extensively delocalized over the protein structure in order to account for the observed dynamics. Collective modes, similar to solid-state lattice phonons, appear to be excited by the doming of the heme ring and play the central role in propagating the tertiary structure changes. There is evidence for a 25-$cm^{-1}$ phonon mode in Mb crystals that has the correct wavelength to match an intramolecular collective protein mode and the right frequency to account for the observed dynamics (*18*). With higher time resolution, the effective frequency of the collective mode responsible for the observed global protein motion can be determined, which should resolve this issue. In addition, studies that use site-directed mutagenesis in the vicinity of the heme should provide important information with respect to the micro-

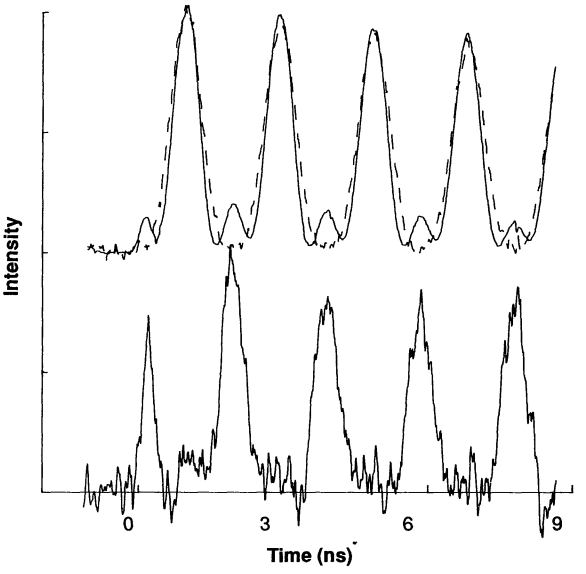


**Fig. 3.** Amplitude of protein displacement for HbCO (top curve, solid line) with a 1064-nm probe at low-excitation energy conditions (1.5 mJ/cm$^2$); the dashed curve is for $HbO_2$. The bottom curve is the response for MbCO under the same experimental conditions.

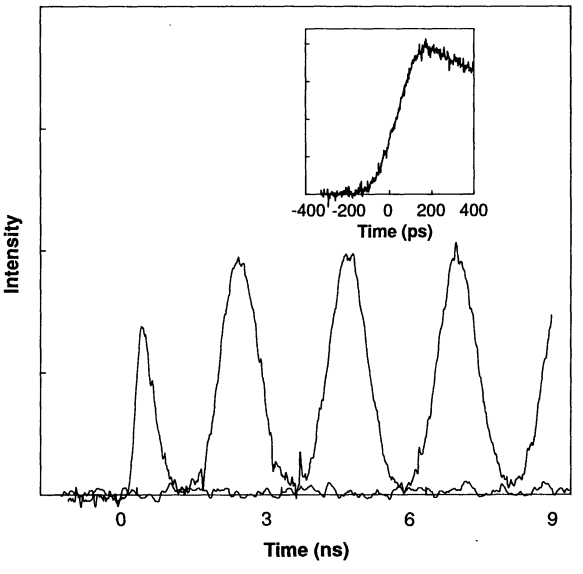


**Fig. 4.** Reduction of the thermal acoustic wave as a function of temperature for Mb. The top curve is for MbCO under intermediate excitation conditions (15 mJ/cm$^2$) at −0.3°C. The bottom curve is for deoxy-Mb under the same experimental conditions. The inset shows the expanded rise time of MbCO at an excitation angle of 2° at room temperature.

scopic coupling to the global structure coordinate.


REFERENCES AND NOTES

1. M. F. Perutz, G. Fermi, B. Luisi, B. Shannan, R. C. Liddington, *Acc. Chem. Res.* **20**, 309 (1987).
2. A. E. Siegman, *J. Opt. Soc. Am.* **67**, 545 (1977); H. J. Eichler, P. Gunter, D. W. Pohl, *Laser-Induced Dynamic Gratings* (Springer-Verlag, Berlin, 1986).
3. K. A. Nelson, R. Casalegno, R. J. D. Miller, M. D. Fayer, *J. Chem. Phys.* **77**, 1144 (1982); H. Kogelnik, *Bell Syst. Tech. J.* **48**, 2909 (1969).
4. R. J. D. Miller, in *Time-Resolved Spectroscopy*, R. J. H. Clark and R. E. Hester, Eds. (Wiley, Chichester, England, 1989), vol. 18, pp. 1–54, and references therein.
5. L. Genberg, Q. Bao, S. Gracewski, R. J. D. Miller, *Chem. Phys.* **131**, 81 (1989); L. Genberg, F. Heisel, G. McLendon, R. J. D. Miller, *J. Phys. Chem.* **91**, 5521 (1987).
6. M. B. Zimmt, *Chem. Phys. Lett.* **160**, 564 (1989).
7. J. W. Petrich, C. Poyart, J. L. Martin, *Biochemistry* **27**, 4049 (1988).
8. P. A. Anfinrud, C. Han, R. M. Hochstrasser, *Proc. Natl. Acad. Sci. U.S.A.* **86**, 8387 (1989).
9. L. P. Murray, J. Hofrichter, E. R. Henry, W. A. Eaton, *Biophys. Chem.* **29**, 63 (1988).
10. W. P. Leung, K. C. Cho, S. K. Chau, C. L. Choy, *Chem. Phys. Lett.* **141**, 220 (1987).
11. J. A. Westrick, K. S. Peters, J. D. Ropp, S. G. Sligar, *Biochemistry* **29**, 6741 (1990).
12. E. R. Henry, W. A. Eaton, R. M. Hochstrasser, *Proc. Natl. Acad. Sci. U.S.A.* **83**, 8982 (1986).
13. A. H. Reynolds, S. D. Rand, P. M. Rentzepis, *ibid.* **78**, 2292 (1981).
14. J. W. Petrich, J. L. Martin, D. Houde, C. Poyart, A. Orszag, *Biochemistry* **26**, 7914 (1987); S. Dasgupta and T. G. Spiro, *ibid.* **25**, 5941 (1986).
15. D. A. Chernoff, R. M. Hochstrasser, A. W. Steele, *Proc. Natl. Acad. Sci. U.S.A.* **77**, 5606 (1980); J. M. Friedman *et al.*, *Science* **229**, 187 (1985).
16. E. W. Findsen, J. M. Friedman, M. R. Ondrias, S. R. Simon, *Science* **229**, 661 (1985); S. M. Janes, G. A. Dalickas, W. A. Eaton, R. M. Hochstrasser, *Biophys. J.* **54**, 545 (1988).
17. A. Ansari *et al.*, *Biochemistry* **25**, 3139 (1986).
18. S. Cusack and W. Doster, *Biophys. J.* **58**, 243 (1990).


19. Supported by NIH grant 1 R01 GM41909-01A1 and an NSF Presidential Young Investigator Award (R.J.D.M.). R.J.D.M. is the recipient of an A. P. Sloan and a Camille and Henry Dreyfus Teacher-Scholar Award.

20 August 1990; accepted 15 November 1990


# Reduction of Deepwater Formation in the Greenland Sea During the 1980s: Evidence from Tracer Data


PETER SCHLOSSER, GERHARD BÖNISCH, MONIKA RHEIN, REINHOLD BAYER



**Hydrographic observations and measurements of the concentrations of chlorofluorocarbons (CFCs) have suggested that the formation of Greenland Sea Deep Water (GSDW) slowed down considerably during the 1980s. Such a decrease is related to weakened convection in the Greenland Sea and thus could have significant impact on the properties of the waters flowing over the Scotland-Iceland-Greenland ridge system into the deep Atlantic. Study of the variability of GSDW formation is relevant for understanding the impact of the circulation in the European Polar seas on regional and global deep water characteristics. New long-term multitracer observations from the Greenland Sea show that GSDW formation indeed was greatly reduced during the 1980s. A box model of deepwater formation and exchange in the European Polar seas tuned by the tracer data indicates that the reduction rate of GSDW formation was about 80 percent and that the start date of the reduction was between 1978 and 1982.**


THE NORTHERN SOURCE OF DEEP water in the world ocean is fed by water flowing over the sills separating the European Polar seas from the Atlantic Ocean. The overflowing waters are produced in the European Polar seas through a complex circulation system that links the Greenland-Iceland-Norwegian seas to the Arctic Ocean (*1, 2*). Deep water formation in the central Greenland Sea plays a key role in this system. Direct contact in this region between the cold water domain and the atmosphere forms the densest part of the potential temperature-salinity sequence observed in the deep waters of the European Polar seas. Recent investigations (*3–5*) indicate that the formation of GSDW was considerably changed during the 1980s. Quantification of the reduction rate has been difficult because of the small signals in temperature and salinity data. Tracer measurements provide a better tool for estimation of the reduction rate of GSDW formation and the time when the GSDW formation rate changed.

Tracer data [concentrations of tritium, $^3$He, and the CFCs F11 ($CCl_3F$) and F12 ($CCl_2F_2$)] have been collected on several cruises to the European Polar seas between 1972 and 1989 (Fig. 1). These data provide sufficient time resolution to study trends in the formation rate of GSDW (*6–12*). For each cruise, we averaged all data below a depth of 1500 m from stations located in the central Greenland Sea. As the hydrographic parameters and the tracer concentrations are homogeneous below this depth (*5, 7, 12, 13*), such a procedure yields a good estimate of the mean tracer concentration of GSDW even in cases where data are available only from single stations. The most remarkable features in the data (Fig. 2) are the increase of the tritium-$^3$He age with time which, for the period between 1979 and 1988, was not significantly different from the one expected for a stagnant water body (indicated by the line in Fig. 2C), and the constant F11 level between 1982 and 1989. Both the linear increase of the tritium-$^3$He age and the constant level of F11 directly indicate that renewal of GSDW slowed considerably during this period. This conclusion is in agreement with the tritium observations between 1979 and 1988, which follow more or less directly the radioactive decay curve calculated for a stagnant water body (Fig. 2A). However, addition of near-surface water is not the only process renewing the deep waters in the Greenland Sea. Exchange with the Arctic Ocean and the Norwegian Sea also contributes to GSDW renewal (*1, 13*). Therefore, we simulated the tracer data with a model designed to estimate the rates of

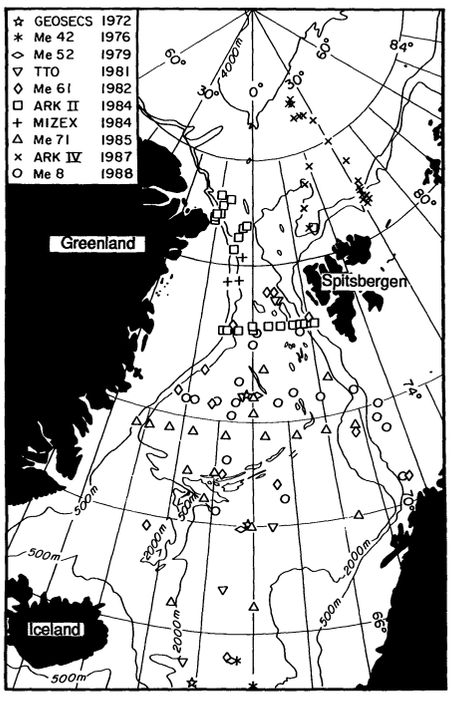


**Fig. 1.** Locations of tritium and $^3$He stations occupied on several cruises (*6*) between 1972 and 1988. The Greenland Sea data used in this study are from cruises GEOSECS, Me42, Me52, TTO, Me62, Me71, and Me8. Only some of the available samples have been measured from Me71 and Me8. Station maps for the CFC stations are in (*5, 11, 12*).


P. Schlosser, Lamont-Doherty Geological Observatory of Columbia University and Department of Geological Sciences, Palisades, NY 10964.
G. Bönisch and R. Bayer, Institut für Umweltphysik der Universität Heidelberg, Im Neuenheimer Feld 366, D-6900 Heidelberg, Germany.
M. Rhein, Institut für Meereskunde an der Universität Kiel, Düsternbrooker Weg 20, D-2300 Kiel, Germany.